Article

Novel #-shaped Fiber-Optic Probe-Based Localized Surface Plasmon Resonance Biosensor for Real-Time Detection of Salmonella Typhimurium

Ya Xu, Zeiwei Luo, Junman Chen, Zhijun Huang, Xu Wang, Huifang An, and Yixiang Duan

Anal. Chem., **Just Accepted Manuscript** • DOI: 10.1021/acs.analchem.8b03905 • Publication Date (Web): 25 Oct 2018

Novel Ω-shaped Fiber-Optic Probe-Based Localized Surface Plasmon Resonance Biosensor for Real-Time Detection of *Salmonella* Typhimurium

Ya Xu,[†] Zewei Luo,[†] Junman Chen,[†] Zhijun Huang,[†] Xu Wang,[‡] Huifang An,[†] Yixiang Duan*[†]

[†]Research Center of Analytical Instrumentation, Key Laboratory of Bio-resource and Eco-environment, Ministry of Education, College of Life Sciences, Sichuan University, Chengdu P. R. China, 610065

[‡]School of Manufacturing Science and Engineering, Sichuan University, Chengdu, P. R. China, 610065

ABSTRACT: A novel, Ω-shaped fiber-optic localized surface plasmon resonance (FOLSPR) biosensor was designed for sensitive real-time and label-free bacteria detection. The designed Ω-shaped fiber-optic probe exhibits an outstanding sensitivity, due to the effect of unique geometry on performance. The results show that refractive index (RI) sensitivity of the Ω-shaped fiber-optic probe is 14 times and 2.5 times higher than those of the straight-shaped and the U-shaped FOLSPR, respectively. In addition, the reason for the geometry and the bending radius effects on RI sensitivity was discussed by investigating the relationship between RI sensitivity and the bending area. The results show that RI sensitivity was enhanced with the increase of bending area, and the best RI sensitivity obtained by Ω-shaped FOLSPR was 64.582 (a.u.)/RIU. Combined with this newly designed Ω-shaped FOLSPR biosensor, a real-time, label-free, sensitive and highly selective bacterial detection method was established. In this work, the aptamers immobilized on the surface of FOLSPR could specifically capture *Salmonella* Typhimurium, resulting in intense change of the absorption peak. In line with this principle, the FOLSPR biosensor achieved high detection sensitivity for *Salmonella* Typhimurium down to 128 CFU/mL within a linear range from 5×10^2 to 1×10^8 CFU/mL, and showed good selectivity for *Salmonella* Typhimurium detection compared to other bacteria. Furthermore, the FOLSPR biosensor was successfully applied to the detection of *Salmonella* Typhimurium in chicken sample with the recoveries of 85–123%. With these characteristics, the novel biosensor is a potential alternative tool in food analysis and environmental monitoring.

As a widely reported gastrointestinal infection bacterium in humans and animals, *Salmonella* has been frequently found to be associated with foodborne diseases outbreaks.[1-5] *Salmonella enteric*. Typhimurium (*Salmonella* Typhimurium) is the originally reported serovar of Salmonella found in human.[6] This bacterium is transmitted by food and has a high mortality rate.[7,8] Additionally, it has strong resistance to the external environment and breeds quickly at normal temperature. Thus, developing an analysis method for sensitive and accurate detection is significant for public health and food safety.

Nucleic acid based molecular assay has been regarded as a gold standard method for highly specific and sensitive detection for bacteria. Nevertheless, its application is limited due to expensive cost, bulk equipment, and complex sample preparation. And the method cannot detect bacterial cells directly, which suffers from the complicated procedures, such as cell lysis and DNA extraction.[9] Recently, some biosensor approaches have been used to detect bacteria, such as surface enhanced Raman scattering (SERS),[10-14] fluorescence biosensors.[15-19] However, they require labeling with external reagents, and the labeling procedure may cause suppression in the specific recognition ability and a high background signal.[20] Label-free detection has become attractive in biosensors. Thus, label-free, inexpensive biosensor based on localized surface plasmon resonance (LSPR) has been developed for bacteria detection.[21,22] Moreover, LSPR has the ability to monitor the binding process of whole bacterial cells in real time, which accounts for another advantage of LSPR.

LSPR is a phenomenon where incident photons and noble metal nanoparticles (MNPs) coherently oscillate with each other. The resonance is associated with MNPs. Especially, gold shows a strong plasmonic effect at the boundary with dielectric materials and therefore it has been widely used to create localized surface plasmon resonance (LSPR)-based sensors.[23] Fiber-optic LSPR (FOLSPR) is based on LSPR using MNPs on a fiber-optic.[24] FOLSPR possesses some advantages including efficient signal delivery, remote sensing, low cost, label-free and real-time detection, and simple installation. However, compared with the traditional fiber-optic surface plasmon resonance (FOSPR), FOLSPR exhibits relatively low sensitivity, which is a big challenge to hinder the further advance of this technique. In the past decade, to deal with this problem, plenty of research efforts have been done to improve the RI sensitivity of FOLSPR by means of changing the kind or size of noble metal nanoparticles.[25-27] However, the strategies focusing on the effect of the natural properties of the fiber-optic on the RI sensitivity is absent in literature.

Apart from above strategies, changing the geometry of fiber-optic probe is another important physical means for RI sensitivity enhancement of FOLSPR sensor. The common straight-shaped FOLSPR has been widely used due to its simple fabrication. However, the straight-shaped FOLSPR is not appropriate for detecting bulky targets, such as bacterial cells, because of its low penetration depth with limited analytical volume.[28] Penetration depth (d_p) is the distance to which the evanescent filed extends beyond the core-cladding interface,[29] which is a key element affecting the RI sensitivity of FOLSPR.[30] Thus, it is necessary to increase penetration depth to improve RI sensitivity. The penetration depth of the evanescent wave in fiber-optic can be increased by modifying the fiber-optic geometry.[29] In past decade, the shape effect on the RI sensitivity of FOLSPR has attracted much attention. Wang's group reported a D-shaped fiber probe prepared by wheel polishing technique, which replaced the complex sample cells with ordinary glass pieces.[31] However, this kind of fiber-optic probe needs to be prepared with the aid of instrument, which makes it difficult to manufacture. Soumyo's Group reported a novel U-shaped fiber-optic probe biosensor based on AuNPs. The fiber-optic probe has the advantages of high RI sensitivity, compact structure, easy preparation and high integration. Our group has reported a series of biosensors based on U-shaped fiber-optic probe in previous works.[32,33] Inspired by the U-shaped fiber-optics, Soumyo and co-workers developed an S-shaped fiber-optic probe,[34] which has a higher RI sensitivity than U-shaped fiber-optic probe. But complex manufacturing processing and sample pool were involved, and large sample volume was required, making it unsuitable for developing biosensor. Importantly, despite of a great deal of studies about the RI sensitivity enhancement of FOLSPR by changing fiber-optics geometry shape, few investigations have been done to reveal the specific mechanism.

Herein, we describe a Ω-shaped FOLSPR for the first time, analyze its RI sensitivity and the related factors, and demonstrate its application as biosensor for bacteria detection. The influence factors on the RI sensitivity of the Ω-shaped FOLSPR are studied from two aspects, namely geometric shape and bending radius. In order to verify the feasibility of the Ω-shaped FOLSPR biosensor, the dynamic process of bacteria detection was monitored using an aptamer-immobilized Ω-shaped FOLSPR-based biosensor. High selectivity and good linearity were obtained, and the linear dynamic range was from 5×10^2 to 1×10^8 CFU/mL with a detection limit of 128 CFU/mL. Therefore, a real-time, label-free, sensitive and specific detection method based on the Ω-shaped FOLSPR biosensor was established, and it is anticipated to be useful for public health and food safety.

Theoretical Background. There are two different media in the structure of fiber-optic: core and cladding. Light propagating through a fiber-optic consists of the guided field in the core and the exponentially decayed evanescent field in the cladding. When light propagating in the fiber-optic, the phenomenon of total internal reflection (TIR) occurs. Thus, there is a critical angle (θ_c) corresponding to the occurrence of TIR, which is expressed as the following equation:

$$\theta_c = \sin^{-1}\left(\frac{n_{cl}}{n_{co}}\right) \quad (1)$$

Where n_{co} and n_{cl} are the refractive indices (RI) of the core and cladding, respectively.

When the cladding is removed, the evanescent filed of the transmitted light is exposed and the light interacts with the surrounding substance of fiber-optic. The distance to which the evanescent filed extends beyond the core-cladding interface is described by d_p. When the cladding is removed, d_p of the fiber-optic is formulated as:

$$d_p = \frac{\lambda}{2\pi\sqrt{n_{co}^2\sin^2\theta - n_s^2}} \quad (2)$$

The θ is the angle of incidence of the light ray, λ is the wavelength of the light source, and n_s is the refractive index (RI) of the surrounding substance.

In early studies, the straight-shaped fiber-optic with the cladding being removed was usually used as probe. When it was used to detect analyte, the analyte adhering on or existing around the fiber-optic core interacts with the evanescent filed, in which the effect of this phenomenon is greatly affected by d_p. In general, the characteristic dimension of bacterial cells is micron sized. According to a previous report, the maximum of d_p in straight fiber probe was about several hundred nanometers.[28] Therefore, the straight fiber-optic probe is not suitable to detect the bacteria, and it is necessary to increase the penetration depth. The penetration depth can be improved by modifying the fiber-optic geometry.[29]

On the other side, according to the wave theory, the properties of light in the fiber core are determined by the number of modes N. Mode and incident angle are one-to-one relationship. Bending area was formed as the geometric shape of the straight fiber-optic changes. An increase in the bending area can increase the times of incident light refraction.[35] This leads to the increase of the kinds of refraction angles, which causes more mode increase. The evanescent filed become stronger as more modes are available. And hence, the increase in evanescent filed is the basis for improve RI sensitivity. Therefore, adjusting the geometry could increase the RI sensitivity.

Accordingly, we designed named Ω-shaped FOLSPR for the first time and compared its RI sensitivity with two other different shaped FOLSPRs, straight-shaped and U-shaped, respectively. It is demonstrated that the Ω-shaped FOLSPR has the highest RI sensitivity.

EXPERIMENTAL SECTION

Reagents. Hydrogen tetrachloroaurate (III) trihydrate ($HAuCl_4 \cdot 3H_2O$), sodium citrate trihydrate ($Na_3C_6H_5O_7 \cdot 3H_2O$), 3-aminopropyltriethoxy silane (3-APTMS), Tris (2-carboxyethyl) phosphine (TCEP), 2-Mercaptoethano, glutaraldehyde were purchased from Sigma-Aldrich (USA) and all were analytical grade. All regents were dissolved in ultrapure water. The *Salmonella* Typhimurium aptamer sequence[36] used was purchased from Sangon Biotech (Shanghai, China) with the sequence of SH-C6-TATGGCGGCGTCACCCGACGGGGACTTGACAT TATGACAG.

Bacterial Strains and Culture Conditions. *Salmonella enterica* Typhimurium (ATCC 14028), *Staphylococcus aureus* (ATCC 6538), *Salmonella enteritidis*, *Escherichia coli* K-12, *Shigella* spp., were kindly provided by West China School of Public Health of Sichuan University. All stains were cultured in Lysogeny broth (LB) at 37 °C under 200 rpm. When growing at log phase for 12 h, the bacteria were collected and saved at -80 ℃ with 25% glycerol for follow-up experiments. The stain concentration was counted by plate counting. Briefly, the bacterial liquid was gradually diluted by sterilized buffer (10 mM Tris-HCl PH 7.4, 5 mM KCl, 100 mM NaCl, 1 mM $MgCl_2$) and incubated onto agar medium at 37 ℃ for 24 h. Then the colonies on the plates were counted out as the number of live bacteria in CFU/mL.

Setup of FOLSPR. A home-made fiber optic LSPR setup consists of tungsten lamp light source (SLS201/M, THORLABS, USA), spectrometer (AvaSpec-ULS2048, Avantes, Netherlands), metal bath (HB120-S, Dragon, China), displacement table (TSA 50-C, Zolix, USA), controller (SC 300-3A, Zolix, USA) and computer, as shown in **Figure 1**. The input end of the FOLPSR probe was connected to a tungsten lamp light source and the output end was connected to a fiber-optic spectrometer. The signal output was carried out on the computer. The metal bath was used to control the temperature. Displacement table was used to control the lifting and lowering of the FOLSPR.

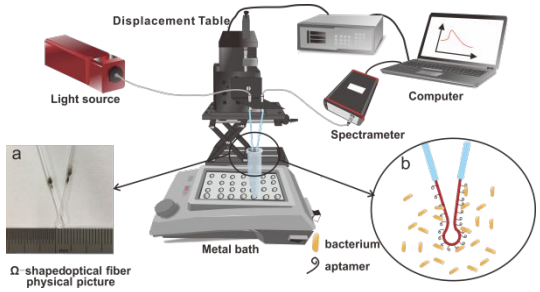

Figure 1 Experimental set-up of the Ω-shaped FOLSPR biosensor. Inset (a) the photo of Ω-shaped fiber-optic; (b) illustration of the combination of bacteria and aptamers.

Synthesis of Gold Nanoparticles. Gold nanoparticles (AuNPs) were prepared according to our previous work.[12] Briefly, 50 ml $HAuCl_4 \cdot 3H_2O$ (0.1 mg/ml) aqueous solution in flask was heated until boiling, and then 0.45 ml 1% (v/v) sodium citrate trihydrate was added into the flask. When the color is stable in wine red, the mixture was kept boiling for 15 min and cooled down to room temperature under stirring.

Fiber-Optic Preparation. The fiber-optic with a silica core in diameter of 600 μm was used in this work. The fiber-optic was cut into 20 cm long pieces. A 2.5±0.2 cm length's cladding in the middle of the fiber-optic was burned off to expose its core. The terminal ends of fiber-optic were polished by using emery papers with 5, 1 and 0.3 μm roughness in sequential order. Then the core of fiber-optic was bended in high temperature flame of alcohol blast burner to get a Ω-shaped fiber-optic as designed (shown in inset of Figure 1(a)). The U-shaped fiber-optic was fabricated by the same processes. The bending radius measured in the experiment was the inner diameter, excluding the diameter of the fiber.

Functionalization of Fiber-Optic Probes. Fiber-optic was functionalized with amino silane for adsorption of AuNPs on the sensor surface. Fiber-optic was dipped in piranha solution (H_2O_2:H_2SO_4=3:7 (v/v)) at 90 ℃ for 30 min, and then washed for 3 times in ultra-pure water. This operation makes hydroxylation of the probe surface to covalently bind amino silane molecules. Fiber-optic was dehydrated at 50 ℃ for 10 min and then was dipped in 1% (v/v) 3-APTMS solution (prepared in the mixture of ethanol and acetic acid in 5:2, v/v) for 15 min. After that, the fiber-optic was sonicated in ethanol for 15 min and in ultra-pure water for 5 min to remove any loosely bound silane. Next, fiber-optic was immersed in synthesized AuNPs solution for 15 min. Functionalized fiber-optic was soaked in 1% glutaraldehyde to block the residual amino and then washed by ultra-pure water. In order to assess the performance, the fiber-optic was immersed into the sucrose solutions with the concentrations of 4%, 8%, 12%, 16%, 20%. AuNPs on the surface of fiber-optic were characterized by TEM (Tecnai G2 F20 S-TWIN, FEI, USA) as shown in **Figure S1**.

Application in *Salmonella* Typhimurium Detection. The fiber-optic probe was applied in the *Salmonella* Typhimurium detection according to the following processes, as shown in

inset (b) of **Figure 1**. Before the detection, the thiol-modified aptamer DNA (1 μM) was activated by 20 mM TCEP for 1 hour to open the disulfide bond and was kept at 95 ℃ for 5 min and slowly annealed to room temperature in 200 μl buffer. Then FOLSPR was immersed into the aptamer DNA solution with high salt concentration (500 mM NaCl) at 37 ℃ for 1 hour. After that, the FOLSPR probe was cleaned with buffer, and immersed into 1.5 ml buffer until the absorption intensity reached stable. Subsequently, different concentrations of bacteria were added into the buffer. In order to investigate the effects of non-target bacteria, *E. coli, Shigella, S. enteritidis and S. aureus* were added into the buffer, respectively. The absorption value was recorded for analysis. In addition, fluorescence experiments were used to more intuitively demonstrate the experimental principle of bacterial binding. In brief, 1 mL *Salmonella* Typhimurium bacteria solution (overnight cultured bacteria) was cleaned three times with buffer under centrifugal at 6600 rpm, and then was concentrated to 100 μL. Subsequently, 10 μg/mL FM4-64 dyes were added to the bacteria solution, on ice, for 1 min. The staining bacteria were bonded to the FOLSPR probe with aptamer for 2 hours and observed under fluorescence microscope (IX83, Olympus, Japan). All combining experiments were performed at 37 ℃.

RESULTS AND DISCUSSION

RI Sensitivity of Different Shape Fiber-Optics. Since RI sensitivity of FOLSPR depends on the geometry of fiber-optic, a novel Ω-shaped FOLSPR was fabricated, and its RI sensitivity was compared with the U-shaped and straight-shaped FOLSPRs. The three kinds of fiber-optics have the same length of decladding area with fiber-optic cores being exposed. These fiber-optic cores were modified by AuNPs with average size around 53 nm as shown in Figure S1. The uniform coating of spherical AuNPs facilitates the generation of LSPR signals.[27] All of the three kinds of FOLSPR were dipped in sucrose solution with different RI from 1.3338 to 1.3639 to obtain the RI sensitivity. According to the previous work, RI sensitivity was defined as the ratio of net absorbance peak to the change in RIU.[37] All of the three kinds of FOLSPR had a linear increase in terms of the maximum absorbance at the fixed wavelength of 530 nm, as shown in **Figure 2A**.The RI sensitivity of the Ω-shaped FOLSPR (red line) was 27.85 (a.u.)/RIU, which was about 2.5 times higher than that of U-shaped FOLSPR (11.18 (a.u.)/RIU) and about 14 times higher than that of straight FOLSPR (1.94 (a.u.)/RIU). Namely, the novel Ω-shaped FOLSPR shows the highest RI sensitivity among the three FOLSPRs with different geometric characteristics. The novel Ω-shaped FOLSPR offers new choice for FOLSPR biosensors.

Bending radius Effect on Ω-shaped FOLSPR. Bending diameter has been proved to be related to the RI sensitivity of U-shaped fiber-optic.[38] So we deduce that the RI sensitivity of the Ω-shaped fiber-optics should be associated with the bending radius. Hence, the Ω-shaped FOLSPR with different bending radii were fabricated and their RI sensitivities were measured. The results are shown in **Figure S2**. RI sensitivity fluctuates around 21 (a.u.)/RIU as the bending radius increase from 0.5 mm to 1 mm. However, for the bending radius over 1 mm, the RI sensitivity increases significantly and fluctuated around 26 (a.u.)/RIU. Based on the theory described above, this may be attributed to few differences in the bending area of the fiber-optic with small bending radius, as the small bending area contributes little to the number of refractions and the modes. After 1 mm, the contribution of the bending area becomes significant, which causes apparent increase in the number of refractions and the modes. Thus, lager bending area of the Ω-shaped FOLSPR takes the advantage of better RI sensitivity. The best RI sensitivity was achieved by the Ω-shaped FOLSPR with the bending radius of 1.25 mm. Hence, the bending radius of 1.25 mm was selected for the following experiments.

Detection of RI Sensitivity of Fiber-Optic Probe Structure. It has been proved by our experimental results that the bending radius and geometry can significantly affect the RI sensitivity of a FOLSPR. However, the detailed mechanism remains unclear. Different bending radii and geometries form different bending areas. Therefore, we deduce that the different areas should have different contributions to the overall RI sensitivity of the optic-fiber probe. To confirm this assumption, the structure RI sensitivity of the U-shaped FOLSPR and the Ω-shaped FOLSPR were investigated at the same time. The signals were obtained with the fiber-optic dropping down into the liquid. The point where the fiber probe first contacts the liquid level was set as the initiate point, and then the signals at dropping depth of 0.5 mm were recorded at the next point. **Figure S3a and S3b** showed the absorption spectra obtained from the FOLSPR immersed at different lengths in water. The absorption spectra in 0-20% (w/v %) sucrose solutions were separately measured, and the absorption intensity at 530 nm of FOLSPR at different immersion depths in different sucrose concentrations are shown in **Figure S3c and S3d**. The results show that the absorption intensity increases as the immersion length of the fiber-optic increased. With the increase of the immersion length of the fiber, the intensity of light lost through the fiber-optic in the solution increased, resulting in an increase in absorbance. Since the relationship between the RI sensitivity and the bending area could not be simply and clearly explained by the absorption intensity, therefore, by fitting linearly between the change of absorbance value and the sucrose RI, the slope of the curve is RI sensitivity here according to description above. And corresponding RI sensitivity were calculated at different immersion lengths. The results are shown in **Figure 2B**. At the beginning, the RI sensitivity decreases as the depth of fiber-optic immersion increased (As shown by S1 in Figure 2B). When the immersion depth reaches S2 stage, the RI sensitivity of the Ω-shaped FOLSPR is significantly increased in the bending areas. At the maximum bending area, where the immersion length is 2.5 mm, the maximum RI sensitivity is 64.583 (a.u.)/RIU, while the RI sensitivity of the U-shaped FOLSPR monotonically decreases in the whole immersion depth range. This is because the bending area of the U-shaped fiber has only one small semicircle, while the Ω-shaped fiber-optic has a nearly full circle. Thereby, the Ω-shaped fiber-optic has larger bending areas than the U-shaped fiber-optic. For the decline of the RI sensitivity of the two types of FOLSPRs, we speculate that there is a complex averaging mechanism. Although the detail mechanism is still unclear, the results show that the RI sensitivity increases significantly in the region where the Ω-shaped FOLSPR has the maximum curvature. According to the above theory, with the increase of the bending areas, both the times of refraction and the modes of light increase, this leads to an increase in the evanescent field. Since the RI sensitivity is usually positively correlated

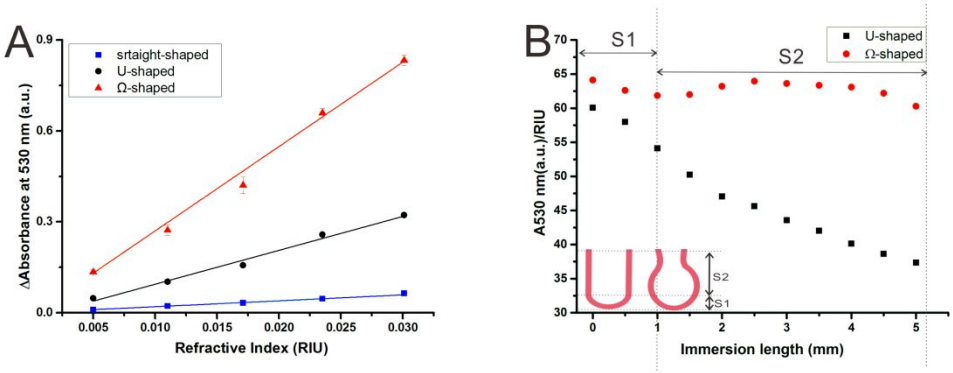

Figure 2. Comparison of RI sensitivity of different shapes of fiber-optics. (A) Compared the RI sensitivity of straight-shaped (■), U-shaped (●) and Ω-shaped (▲) FOLSPR. A linear relationship between the absorbance responses and RI was obtained. The RI sensitivity of Ω-shaped, U-shaped and straight-shaped FOLSPR were 27.85 (a.u.)/RIU, 11.18 (a.u.)/RIU and 1.95 (a.u.)/RIU with R^2 =0.996, 0.980 and 0.999, respectively. The net absorbance value is calculated by A_s-A_w (A_s for absorbance value in sucrose, A_w for absorbance value in water). Error bars represent standard deviation (n=3). (B) The structural RI sensitivity of 600 μm core diameter of U-shaped and Ω-shaped FOLSPR. Measure one point for every 0.5 mm drop. The inserted picture is a schematic of U-shaped and Ω-shaped FOLSPR. S1 and S2 in the schematic represent the length of the fiber in the immersion solution, corresponding to the RI sensitivity

with the evanescent field, as the performance of the Ω-shaped FOLSPR shows, the increasing of the bending area can effectively improve the RI sensitivity of FOLSPR. However, we also found that the LSPR signal will be unstable when there are too many bending areas, which leading to the difficulty of data collection. As shown in Figure S4, absorption intensity of FOLSPR was fluctuated up and down when the optic-fibers were bending into the 8-shaped or the spiral-shaped. For the spiral-shaped FOLSPR, the fluctuations have exceeded the limits of the spectrometer, making the data invalid. For the 8-shaped FOLSPR, the fluctuations have a range of -0.1 to 0.1, this wide fluctuation will interfere with bacterial monitoring. In addition, the preparation process of the both two shaped optic-fibers mentioned above is much more difficult than the Ω-shaped one. In contrast, the Ω-shaped FOLSPR has both sensitive and stable characteristics, which are beneficial to biosensor applications. The mechanism study of the increased RI sensitivity in FOLSPR proved that the bending area is the determinant of the RI sensitivity of the FOLSPR, which can provide a simple way to enhance the RI sensitivity of the FOLSPR.

Application of the Ω-shaped FOLSPR in Bacterial Detection. After demonstration of its good performance, the Ω-shaped FOLSPR was further used to design a biosensor for bacterial detection. In order to construct a label-free FOLSPR sensor for *Salmonella* Typhimurium detection, an aptamer with highly specificity and affinity[36,39,40] was chosen to modify the surface of fiber-optic as mentioned in the experiment section. The process of aptamer immobilization was monitored in real time by the Ω-shaped FOLSPR, as shown in **Figure S5**. The FOLSPR combined with an aptamer is called FOLSPR probe. The thiol-modified aptamer sequence was selected for bacterial detection because the combination of thiol groups and AuNPs forms Au-S bonds that allow the aptamer to be stably immobilized on the surface of the fiber-optic. The absorption spectra obtained from different aptamer binding time are shown in **Figure S5a**. The experimental results show that the absorbance increases as more aptamers bind to the fiber-optic surface. From **Figure S5b**, apparent increase in absorption was observed at the initial stage, indicating a large amount of aptamers was rapidly bound to the fiber optic surface. Then the absorption was close to saturation after reaction for 20 min. Therefore, 20 min was selected as the optimal time for the following experiments. To verify the specificity of the aptamer to *Salmonella* Typhimurium, the fluorescence imaging was carried out firstly with random DNA sequence as control group. As shown in **Figure 3**, *Salmonella* Typhimurium was well captured by the FOLSPR probe modified with aptamers, while little *Salmonella* Typhimurium was captured in the control group. These results demonstrate that the aptamer is highly specific and affinity is suitable for binding *Salmonella* Typhimurium. As shown in **Figure 4**, adding bacteria after 5 min of equilibration, the generated signal increased with the increase of the detected concentration of *Salmonella* Typhimurium. In low concentration ranges, the absorbance slowly rises, which implies that the bacteria slowly bind to the aptamer. At high concentrations, the absorbance rapidly rises, which is caused by the bacteria binding in large amounts. After 100 min, there was no significant upward trend in the concentration range examined, hence, 100 min was chosen as the optimal binding time. The absorption intensity at 530 nm has a linear relationship with the detected *Salmonella* Typhimurium concentrations from 5×10^2 CFU/mL to 1×10^8 CFU/mL and a

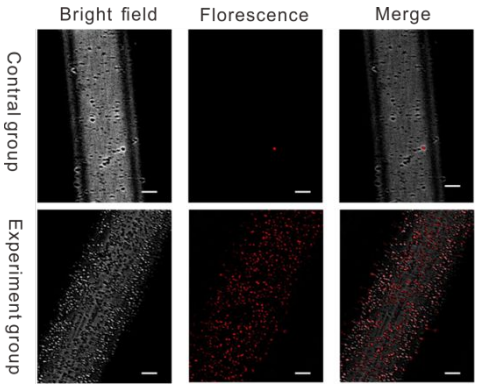

Figure 3. Experimental principle verification of the Ω-shaped FOLSPR biosensor for *Salmonella* Typhimurium detection. Picture was taken at 4× microscope.

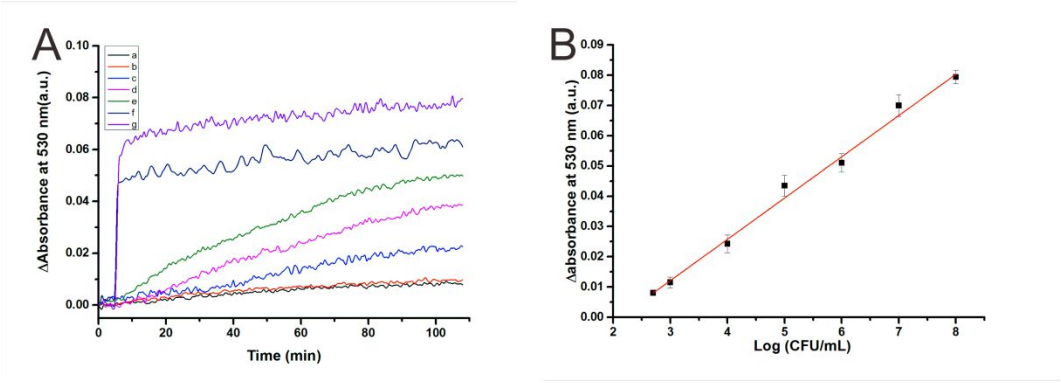

Figure 4. The sensitivity of the developed biosensor for *Salmonella* Typhimurium detection. (A) The result of different concentrations of *Salmonella* Typhimurium on the LSPR response: (a) 5×10^2 CFU/mL, (b) 1×10^3 CFU/mL (c) 1×10^4 CFU/mL, (d) 1×10^5 CFU/mL, (e) 1×10^6 CFU/mL (f) 1×10^7 CFU/mL and (g) 1×10^8 CFU/mL. (B) Linear relationship between the change of the absorbance intensity and the concentration of *Salmonella* Typhimurium on logarithmic scales.

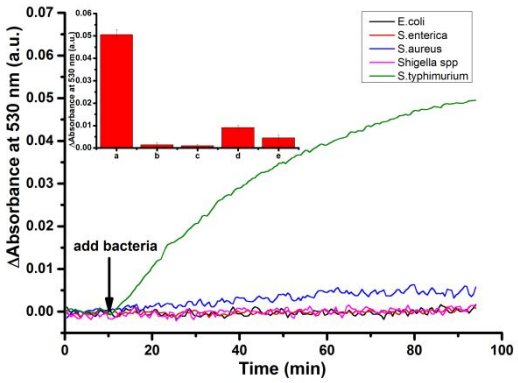

Figure 5. Selectivity evaluation of the proposed biosensor. In histogram (a) *Salmonella* Typhimurium (b) *E. coli* (c) *S. enterica* (d) *S. aureus* and (e) *Shigella*. The concentrations of bacteria were all 10^6CFU/mL. The error bars were standard deviations of three repetitive measurements. The arrow shows the time of bacteria addition.

limit of detection (LOD) of 128 CFU/mL were finally achieved (LOD was calculated by the formula of LOD=3σ/S, in which σ represents the standard deviation of the blank, and the S denotes the slope of the linear curves.). Such a detection limit is significantly improvedwhen comparing with the other reported biosensors for *Salmonella* Typhimurium detection.[18,41] Additionally, the performances of the U-shaped FOLSPR probe and the Ω-shaped FOLSPR probe for *Salmonella* Typhimurium detection was compared at the concentration of 10^6 CFU/mL (**Figure S6**). Obviously, the sensitivity of the Ω-shaped FOLSPR probe is higher than that of the U-shaped FOLSPR probe. According to these results, the Ω-shaped FOLSPR biosensor enables real-time, label-free and sensitive monitoring of *Salmonella* Typhimurium.

The high selectivity of aptamer for *Salmonella* Typhimurium confirmed by gel electrophoresis (**Figure S7a**) and fluorescence (**Figure S7b**) experiments, respectively. But these two methods were only qualitative analysis. To further prove the selectivity, 10^6 CFU/mL *S. aureus, E. coli, S. enteritis, Shigella* and *Salmonella* Typhimurium were detected with the FOLSPR biosensor under identical conditions. The results are shown in **Figure 5.** Add bacteria when the reaction reached equilibrium 10 min, there was no significant absorption intensity increment upon the addition of non-target bacteria except *Salmonella* Typhimurium. These results demonstrate that the Ω-shaped FOLSPR was selective for *Salmonella* Typhimurium. The excellent specificity obtained with the strategy is attributed to the good selectivity and high affinity of the aptamer against *Salmonella* Typhimurium.

Real Sample Application in Chicken. For assessing the feasibility and the potential application of the proposed assay, a piece of chicken was added aseptically to a beaker, mixed with buffer for 1 hour and took out the supernatant to inoculate with various concentrations of *Salmonella* Typhimurium. Then, the liquid with *Salmonella* Typhimurium was taken as sample for analysis by the proposed Ω-shaped FOLSPR biosensor. Using chicken samples without *Salmonella* Typhimurium as a blank, the recoveries and relative standard deviations (RSDs) varied from 85% to 123% and 6.5% to 8.3%, respectively. This indicates that the novel Ω-shaped FOLSPR biosensor strategy based on the aptamer has a good detection performance in practical application.

Table 1. Application of the proposed biosensor for *Salmonella* Typhimurium detection in chicken samples.

Sample	*Salmonella* Typhimurium added (CFU/mL)	Detected by the biosensor (CFU/mL)	Recovery (%)	RSD (%)
1	1.0×10^5	0.93×10^5	93	7.9
2	1.0×10^6	0.85×10^6	85	6.5
3	1.0×10^7	1.23×10^7	123	8.3

CONCLUSION

In summary, we propose a novel Ω-shaped fiber-optic probe that shows better performance compared with the U-shaped or

the straight-shaped fiber-optic probes. This biosensor enables sensitive, label-free, real-time detection and has a wide linear range. It is thus expected that this novel Ω-shaped FOLSPR biosensor can be developed into a potentially versatile system for direct detection of a large number of pathogenic bacteria and other objects of interest such as cancer cells simply by altering the corresponding object recognition probes. Nevertheless, the detailed mechanism of the RI sensitivity increase in FOLSPR is not clear yet so far. Thus, further in-depth studies are needed to reveal the mechanism of RI sensitivity enhancement in FOLSPR biosensors.

ASSOCIATED CONTENT

Supporting Information

The Supporting Information is available free of charge on the ACS Publications website.
Additional figures (PDF)

AUTHOR INFORMATION

Corresponding Author

*E-mail address: yduan@scu.edu.cn

Author Contributions

The manuscript was written through contributions of all authors. All authors have given approval to the final version of the manuscript.

Notes

The authors declare no competing financial interest.

ACKNOWLEDGMENT

This research was gratefully supported by the National Natural Science Foundation of China (No. 21874095), the Key Research and Development Project from Department of Science and Technology, Sichuan Province (2017SZ0013) PR China, and Graduate Student's Research and Innovation Fund of Sichuan University (No. 2018YJSY054).

REFERENCES

(1) Li, K.; Ye, S.; Alali, W. Q.; Wang, Y.; Wang, X.; Xia, X.; Yang, B. *Food Control* **2017**, *72*, 36-42.
(2) De, K. L. V.; Pires, S. M.; Hald, T. *Epidemiol. Infect.* **2015**, *143*, 1175-1186.
(3) Finstad, S.; O'Bryan, C. A.; Marcy, J. A.; Crandall, P. G.; Ricke, S. C. *Food Res. Int.* **2012**, *45*, 789-794.
(4) Zweifel, C.; Stephan, R. *Food Res. Int.* **2012**, *45*, 765-769.
(5) Hoffmann, M.; Luo, Y.; Monday, S. R.; Gonzalesescalona, N.; Ottesen, A. R.; Muruvanda, T.; Wang, C.; Kastanis, G.; Keys, C.; Janies, D. *J. Infect. Dis.* **2015**, *213*, 502-508.
(6) Yuan, J.; Tao, Z.; Yu, Y.; Ma, X.; Xia, Y.; Wang, L.; Wang, Z. *Food Control* **2014**, *37*, 188-192.
(7) Hawkey, J.; Edwards, D. J.; Dimovski, K.; Hiley, L.; Billmanjacobe, H.; Hogg, G.; Holt, K. E. *Bmc. Genomics* **2013**, *14*, 800.
(8) Greene, S. K.; Stuart, A. M.; Medalla, F. M.; Whichard, J. M.; Hoekstra, R. M.; Chiller, T. M. *Foodborne Pathog. Dis.* **2008**, *5*, 669-680.
(9) Zhang, P.; Liu, H.; Li, X.; Ma, S.; Men, S.; Wei, H.; Cui, J.; Wang, H. *Biosens Bioelectron* **2016**, *87*, 1044-1049.
(10) Wang, H.; Zhou, Y.; Jiang, X.; Sun, B.; Zhu, Y.; Wang, H.; Su, Y.; He, Y. *Angew. Chem. Int. Ed.* **2015**, *54*, 5132-5136.
(11) Zhang, H.; Ma, X.; Liu, Y.; Duan, N.; Wu, S.; Wang, Z.; Xu, B. *Biosens Bioelectron* **2015**, *74*, 872-877.
(12) Ma, X.; Xu, X.; Xia, Y.; Wang, Z. *Food Control* **2017**, *84* 232-237.
(13) Zhou, H.; Yang, D.; Ivleva, N. P.; Mircescu, N. E.; Niessner, R.; Haisch, C. *Anal. Chem*. **2012**, *86*, 1525-1533.
(14) Zhang, L.; Xu, J.; Mi, L.; Gong, H.; Jiang, S.; Yu, Q. *Biosens Bioelectron* **2012**, *31*, 130-136.
(15) Zhou, S.; Pi, X.; Ni, Z.; Ding, Y.; Jiang, Y.; Jin, C.; Delerue, C.; Yang, D.; Nozaki, T. *Acs Nano* **2015**, *9*, 378-386.
(16) Zhang, P.; Liu, H.; Li, X.; Ma, S.; Men, S.; Wei, H.; Cui, J.; Wang, H. *Biosens Bioelectron* **2016**, *87*, 1044-1049.
(17) Yu, M.; Wang, H.; Fu, F.; Li, L.; Li, J.; Li, G.; Song, Y.; Swihart, M. T.; Song, E. *Anal. Chem*. **2017**, *89*, 4085-4090.
(18) Kim, J. Y.; Sahu, S.; Yau, Y. H.; Wang, X.; Shochat, S. G.; Nielsen, P. H.; Dueholm, M. S.; Otzen, D. E.; Lee, J.; Delos Santos, M. M. Journal of the *J. Am. Chem. Soc.* **2015**, *138*, 402-407.
(19) Rhee, H. W.; Lee, C. R.; Cho, S. H.; Song, M. R.; Cashel, M.; Choy, H. E.; Seok, Y. J.; Hong, J. I. *J. Am. Chem. Soc.* **2008**, *130*, 784-785.
(20) Endo, T.; Kerman, K.; Nagatani, N.; Yuzuru Takamura, A.; Tamiya, E. *Anal. Chem*. **2005**, *77*, 6976-6984.
(21) Hu, J.; Fu, K.; Bohn, P. W. *Anal. Chem*. **2018**, *90*, 2326-2332.
(22) Yoo, S. M.; Kim, D. K.; Sang, Y. L. *Talanta* **2015**, *132*, 112-117.
(23) Tu, M. H.; Sun, T.; Grattan, K. T. V. *Sens. Actuators B Chem*. **2014**, *191*, 37-44.
(24) Jeong, H. H.; Erdene, N.; Park, J. H.; Jeong, D. H.; Lee, H. Y.; Lee, S. K. *Biosens Bioelectron* **2013**, *39*, 346-351.
(25) Mitsushio, M.; Miyashita, K.; Higo, M. *Sensor Actuat. A-Phys.* **2006**, *125*, 296-303.
(26) Sepúlveda, B.; Angelomé, P. C.; Lechuga, L. M.; Liz-Marzán, L. M. *Nano Today* **2009**, *4*, 244-251.
(27) Tu, M. H.; Sun, T.; Grattan, K. T. V. *Sens. Actuators B Chem*. **2012**, *164*, 43-53.
(28) Nath, N.; Chilkoti, A. *Anal. Chem*. **2004**, *76*, 5370-5378.
(29) Leung, A.; Shankar, P. M.; Mutharasan, R. *Actuators B Chem*. **2007**, *125*, 688-703.
(30) Wandermur, G.; Rodrigues, D.; Allil, R.; Queiroz, V.; Peixoto, R.; Werneck, M.; Miguel, M. *Biosens Bioelectron* **2014**, *54*, 661-666.
(31) Zhao, J.; Cao, S.; Liao, C.; Wang, Y.; Wang, G.; Xu, X.; Fu, C.; Xu, G.; Lian, J.; Wang, Y. *Sens. Actuators B Chem*. **2016**, *230*, 206-211.
(32) Liang, G.; Zhao, Z.; Wei, Y.; Liu, K.; Hou, W.; Duan, Y. *Rsc Advances* **2015**, *5*, 23990-23998.
(33) Luo, Z.; Zhang, J.; Wang, Y.; Chen, J.; Li, Y.; Duan, Y. *Sens. Actuators B Chem*. **2016**, *236*, 474-479.
(34) Chauhan, S.; Punjabi, N.; Sharma, D.; Mukherji, S. *Procedia Engineering* **2016**, *168*, 117-120.
(35) Bharadwaj, R.; Sai, V. V.; Thakare, K.; Dhawangale, A.; Kundu, T.; Titus, S.; Verma, P. K.; Mukherji, S. *Biosens Bioelectron* **2011**, *26*, 3367-3370.
(36) Joshi, R.; Janagama, H.; Dwivedi, H. P.; Senthil Kumar, T. M.; Jaykus, L. A.; Schefers, J.; Sreevatsan, S. Molecular and cellular probes 2009, 23, 20-28.
(37) Sai, V. V.; Kundu, T.; Mukherji, S. Biosens Bioelectron 2009, 24, 2804-2809.
(38) Khijwania, S. K.; Gupta, B. D. *Opt. Commun.* **2000**, *175*, 135-137.
(39) Labib, M.; Zamay, A. S.; Kolovskaya, O. S.; Reshetneva, I. T.; Zamay, G. S.; Kibbee, R. J.; Sattar, S. A.; Zamay, T. N.; Berezovski, M. V.; Chem, A. *Anal. Chem*. **2012**, *84*, 1813-1816.
(40) Thiha, A.; Ibrahim, F.; Muniandy, S.; Dinshaw, I. J.; Teh, S. J.; Thong, K. L.; Leo, B. F.; Madou, M. *Biosens Bioelectron* **2018**, *107*, 145-152.
(41) Guo, P. L.; Tang, M.; Hong, S. L.; Yu, X.; Pang, D. W.; Zhang, Z. L. *Biosens Bioelectron* **2015**, *74*, 628-636

Table of contents